Tunable electromagnetically induced transparency and absorption with dressed superconducting qubits

Hou Ian,[1] Yu-xi Liu,[1,2,3] and Franco Nori[1,4]
[1]*Advanced Science Institute, RIKEN, Wako-shi, Saitama 351-0198, Japan*
[2]*Institute of Microelectronics, Tsinghua University, Beijing 100084, China*
[3]*Tsinghua National Laboratory for Information Science and Technology (TNList), Tsinghua University, Beijing 100084, China*
[4]*Physics Department, The University of Michigan, Ann Arbor, Michagan 48109, USA*
(Received 2 December 2009; published 23 June 2010)

Electromagnetically induced transparency and absorption (EIT and EIA) are usually demonstrated using three-level atomic systems. In contrast to the usual case, we theoretically study the EIT and EIA in an equivalent three-level system: a superconducting two-level system (qubit) dressed by a single-mode cavity field. In this equivalent system, we find that both the EIT and the EIA can be tuned by controlling the level-spacing of the superconducting qubit and hence controlling the dressed system. This tunability is due to the dressed relaxation and dephasing rates which vary parametrically with the level-spacing of the original qubit and thus affect the transition properties of the dressed qubit and the susceptibility. These dressed relaxation and dephasing rates characterize the reaction of the dressed qubit to an incident probe field. Using recent experimental data on superconducting qubits (charge, phase, and flux qubits) to demonstrate our approach, we show the possibility of experimentally realizing this proposal.

DOI: 10.1103/PhysRevA.81.063823 PACS number(s): 42.50.Gy, 42.65.An, 85.25.−j

I. INTRODUCTION

A. Electromagnetically induced transparency in optics and superconducting circuits

Electromagnetically induced transparency (EIT) [1,2] manifests spectroscopically the quantized three-level structure of an atomic medium through its interactions with two semiclassical fields. It has been widely explored in various contexts (e.g., [3–6]) since its inception. For example, the EIT effect has been studied in the context of a two-level atom [6], instead of the usual three-level system. In Ref. [6], the energy levels of the atom are split by a driving optical field into doublets, equivalent to ac Stark shifts, and the transparency is realized on the final four-level system.

The development of superconducting quantum circuits (SQCs) in recent years has heavily employed concepts from quantum optics, and SQCs have become a testbed of quantum optical phenomena, including EIT (e.g., [7–9]). In one case [7], a flux qubit system has even taken advantage of the EIT effect as a means to probe decoherence by circling the flux qubit with a readout superconducting quantum interference device (SQUID) in the SQC. Both the optical version and the SQC version of the EIT effect are illustrated on the left and right panels, respectively, of Fig. 1, to compare their similarity and differences. This also serves as a prelude to our discussion of the tunability of electromagnetically induced transparency and absorption.

For the optical version, on the left of Fig. 1, two different kinds of classical electromagnetic waves, $\Omega_p(t) = \Omega_p e^{-i\omega_p t}$ and $\Omega_c(t) = \Omega_c e^{-i\omega_c t}$, are shown, for a typically weak probe field $\Omega_p(t)$ and a strong control field $\Omega_c(t)$ (where $\Omega_c \ll \Omega_p$). These are shown incident on an optical medium in Figs. 1(a) and 1(b), respectively. The frequencies, ω_p and ω_c, of these two fields are resonant with some energy level spacings of the optical medium, which are typically Λ-type three-level atoms, and each of these two fields alone will be absorbed and cannot travel through the medium. Figure 1(g) shows a canonical level diagram for such three-level atoms, where the probe field is resonant with the level spacing between $|1\rangle$ and $|3\rangle$ and the control field with that between $|2\rangle$ and $|3\rangle$.

When the probe and control fields are simultaneously incident on the medium, as shown in Fig. 1(c), the resonance between the control field and the medium will render the medium detuned from the probe field and hence let the probe field travel through without being absorbed. Level $|3\rangle$ is driven out of its original position from $|2\rangle$ and makes the $|1\rangle$-to-$|3\rangle$ spacing detuned from the probe field frequency in Fig. 1(g). In other words, an absorbing medium becomes transparent to an incident probe field when a control field is simultaneously applied. More precisely, the transparency of the probe field can be considered as an effect of its quantum interference with the control field. The strong coupling of the medium with the control field perturbs the original level spacings and provides two excitation pathways of equal probability but opposite signs to the probe field, indicated by the Autler-Townes levels $|3+\rangle$ and $|3-\rangle$ in Fig. 1(g). The resulting signal that exits from the medium is thus a destructive superposition of two versions of the same signal, and hence a destructive interference and a zero-absorption of the linear susceptibility (see, e.g., [2] for a comprehensive review). Note that in the atypical case where both the probe and the control are strongly coupled to the medium, the interference pattern is severely altered: In one case, simultaneous transparency for both fields is achieved [10] whereas, in another, an enhanced absorption of the probe can occur [11].

The SQC version of the optical EIT is illustrated on the right side of Fig. 1, where the optical medium is replaced by a Josephson-junction multilevel system. In a similar manner, when the probe and the control signals $\Omega_p^{in}(t)$ and $\Omega_c^{in}(t)$, which are either current or voltage signals in this case, are fed separately into the SQC [shown in Figs. 1(d) and 1(e)], the amplitudes of their outputs $\Omega_p^{out}(t)$ and $\Omega_c^{out}(t)$ will be smaller than those of their inputs. This shows that the SQC

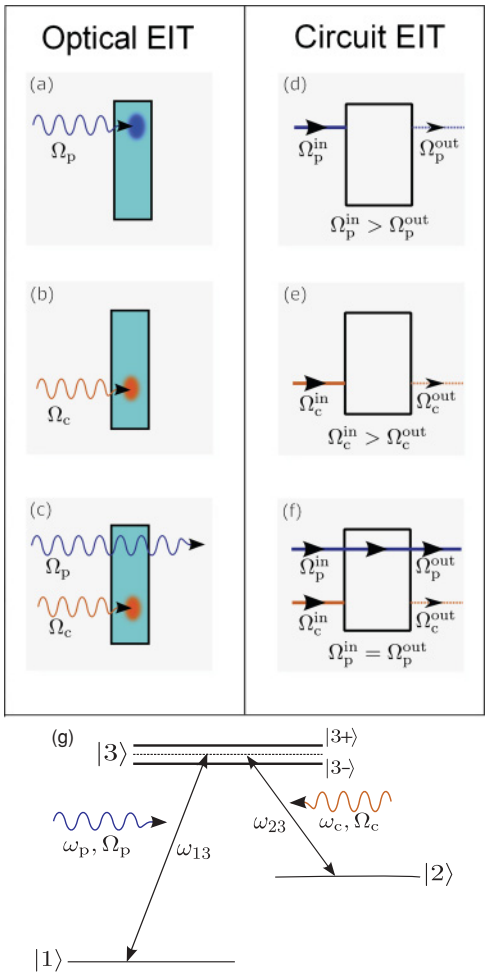

FIG. 1. (Color online) Schematic diagram illustrating electromagnetically induced transparency. Panel (a) schematically shows a medium that strongly absorbs a probe light beam of amplitude Ω_p; (b) shows the same absorption, but for a control light beam of amplitude Ω_c. However, when both beams are applied simultaneously, as in (c), then the previously absorbing medium becomes transparent for the probe beam Ω_p (i.e., transparency is electromagnetically induced by the control field Ω_c). The superconducting circuit analog of this phenomenon is schematically shown in (d), (e), and (f), where a "box" schematically represents the circuit. In (d) a classical voltage or current signal (in the microwave range) of amplitude Ω_p^{in} is fed into the input of the circuit. The signal is "absorbed" in the circuit and the amplitude Ω_p^{out} of the output signal is less than that of the input. Panel (e) shows the same effect with another microwave control signal of amplitude Ω_c. However, when *both* microwave signals are applied simultaneously to the circuit, as in (f), then the previously "absorbing medium," now a circuit, becomes *transparent* for the first signal Ω_p^{in}. Panel (g) shows a canonical level diagram for a three-level system coupled to a weak probe field and a strong control field.

separately absorbs the input signals due to resonances between the input electrical signals and the energy level spacings of the Josephson-junction device. Nonetheless, a *simultaneous* application of the *two* input signals would let the probe signal conduct through the circuit *without* losing energy, while the control signal is mostly absorbed, as shown in Fig. 1(f).

B. Electromagnetically induced absorption

Two closely related, but far less studied, optical phenomena are electromagnetically induced absorption (EIA) [12] and switchable dispersion [13], where the hyperfine structure of the ground state of an atom is used. The quasi- or near-degenerate levels originate from the same ground-state hyperfine level and have a very small splitting; when the configurations of their total angular momentum and that of their excited state have even parity, a Δ-type three-level system with closed cyclic transitions is formed. In contrast to the odd-parity case, where the three-level system becomes of Λ type and can exhibit EIT, the even-parity configuration makes the multilevel medium absorptive to the probe field even when it is resonant with the control field. These relations between optical properties and the parities of SQCs were recently predicted theoretically [14] and verified experimentally [15] based on selection rules and symmetry breaking.

C. Tunable transparency and absorption

The circuit designs in Refs. [7,8] are based on the multilevel energy structure of Josephson-junction devices. These designs require advanced measurement techniques where the third and higher energy levels are often far separated from the bottom two. We therefore consider in this article an alternative way to construct a multilevel energy structure in SQCs by "mixing" a two-level system with a resonant field, forming a dressed multilevel structure that is tunable and does not entirely rely on the device characteristics of the junctions.

Considering the recent progress in studies on superconducting qubits (e.g., [16–20]) and dressed superconducting qubits by a single-mode cavity field [21,23], we study here a dressed three-level qubit equivalent to those in three-level Josephson-junction devices, in order to theoretically realize the effect of EIT on SQCs. Also motivated by the studies of EIT and EIA in atomic systems (e.g., [1,6,12,13]), we show how the EIT and the EIA phenomena coexist and transmute into each other on the same dressed SQC.

We will select three energy levels among the multiple levels of the dressed superconducting qubit. The tunable level spacing of the superconducting qubit then not only affects the level splitting of the dressed states but also affects the relaxation and dephasing rates of the dressed system. These tunable relaxation and dephasing rates will determine the system's specific dynamics when coupled to a classical signal field, effectively making it have either a Δ-type (closed) or a Λ-type (open) transition pattern. Therefore, if two classical electromagnetic fields, the probe field and the control field, are fed concurrently into the circuit, the complex susceptibility of the dressed qubit gives an absorption spectrum that either dips or peaks at the zero probe field detuning. The choice of dip or peak of the spectrum is analytically determined by a biquadratic equation which is dependent on the qubit level spacing and the environment temperature through the dressing process. By determining the number of real roots given by this equation, we can distinguish two effective regimes of operations: EIT and EIA.

The dip-type and the peak-type spectra correspond to the EIT and the EIA effect, respectively, depending on the magnitude of the qubit level spacing with respect to the

eigenfrequency of the resonator quantum field. Compared to the atomic case, the lower two dressed states from the superconducting qubit hence act like those hyperfine levels from the atomic ground state, giving either a closed transition for the EIA regime or an open transition for the EIT regime. Note also that these tunable regimes of operations are closely related to the tunable luminosity suggested by Agarwal *et al.* [22], where the group velocity of light is controlled by a "knob" signal field that couples the metastable states. The tunable metastable-state coupling given effectively by our dressing process is thus comparable to that given directly through the knob field.

Our analysis will focus on superconducting quantum circuits that have a strong coupling between the qubit and the resonator [24,25], realized by a coplanar waveguide (CPW) transmission line. These circuits include combinations of the CPW resonator with a charge qubit [23,26,27], a phase qubit [28–30], or a flux qubit [31].

In Sec. II, we first describe a general theoretical model and derive the energy spectrum of the dressed multilevel system. The dressing process is described in Sec. III. The first-order susceptibility and the dressed relaxation and dephasing rates among the multiple levels of the qubit-resonator combination are calculated in Sec. IV using a density matrix formulation. The determination of the switching between the transparency and the absorption as well as the discussion of the corresponding transition patterns are presented in Sec. VI. In Sec. VII, we then consider experimentally accessible parameters for different types of qubits to demonstrate and numerically analyze our theoretical results. Conclusions are summarized in Sec. VIII.

II. UNDRESSED QUBIT

Our discussion of the superconducting qubit system is independent of the specific type of qubits (phase qubit, charge qubit, or flux qubit) employed. Because the two-level structures of these qubits are commonly described by a general Hamiltonian with a σ_z term and a σ_x term [16–19]. To simplify our discussion, here we consider the qubit in the diagonal basis whose eigenfrequency ω_q is the root mean square of the coefficients of the σ_z and σ_x terms. The CPW resonator that couples to the qubit, akin to a cavity for photons, is described by a pair of annihilation and creation operators a and $a^\dagger$ with a resonant frequency denoted by ω_0. The dipole-field coupling between the qubit, acting as the dipole, and the energy quantum within the CPW resonator, acting as the cavity field, is along the z direction of the qubit in the nondiagonal basis. In the diagonal basis of the qubit, the Hamiltonian between the qubit and the transmission-line resonator is given by the Jaynes-Cummings model

$$H_{\rm cir} = \omega_q \sigma_z + \omega_0 a^\dagger a + \eta(a^\dagger \sigma_- + a\sigma_+), \tag{1}$$

with a rotating-wave approximation and $\hbar = 1$, where η denotes the coupling constant between the cavity field and the qubit. Here, for convenience, we still use σ_z to denote the qubit operator in the diagonal basis.

Two signals, the probe signal and the control signal, with traveling frequencies denoted by $\omega_{\rm p}$ and $\omega_{\rm c}$ and Rabi frequencies denoted by $\Omega_{\rm p}$ and $\Omega_{\rm c}$, respectively, are fed into the circuit. These two signals are treated as classical

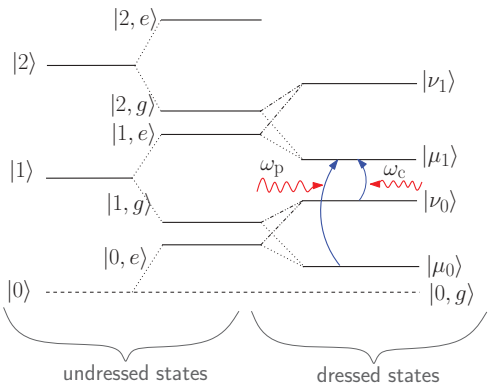

FIG. 2. (Color online) Schematic diagram of the "dressing" process. The Fock number states $|n\rangle$ of a coplanar-waveguide resonator (shown in the first column) as well as the ground state $|g\rangle$ and excited state $|e\rangle$ of a qubit provide the "undressed" tensor-product states $|n,g\rangle$ and $|n,e\rangle$ (shown on the middle column). These tensor states are modified by their mutual interaction, producing the renormalized or "dressed" states $|\mu_n\rangle$ and $|\nu_n\rangle$ (shown on the right). Mathematically, these states correspond to the eigenvectors of the circuit Hamiltonian in a nondiagonal basis (undressed states) and the diagonal basis (dressed states), respectively.

electromagnetic fields and their interaction Hamiltonian with the qubit can be written as

$$H_{\rm ext} = \Omega_{\rm p} e^{i\omega_{\rm p} t}\sigma_- + \Omega_{\rm c} e^{i\omega_{\rm c} t}\sigma_- + {\rm H.c.} \tag{2}$$

The total system Hamiltonian is then given by

$$H = H_{\rm cir} + H_{\rm ext}. \tag{3}$$

The energy states of the CPW resonator and the qubit before dressing are shown as horizontal lines on the left part of the schematic diagram in Fig. 2. Note that the energy levels $|n,g\rangle$ and $|n,e\rangle$ have equal spacings for all n: For fixed probe field and control field, the undressed qubit with a particular level spacing might not resonate with them. Having been *dressed* (a process to be discussed in next section) by the CPW resonator, the qubit will exhibit a spectrum with numerous energy levels spaced in a tunable nonuniform pattern, as shown on the right part in Fig. 2, providing more possibilities for matching levels between the dressed qubit and the probe and control signals.

III. DRESSED QUBIT

The dressed qubit Hamiltonian can be derived by rewriting the Jaynes-Cummings model, which usually describes the atom-photon coupling for the circuit Hamiltonian $H_{\rm cir}$ in Eq. (1). Note that the set $\{|n,e\rangle, |n+1,g\rangle\}$ spans an invariant subspace V_n of $H_{\rm cir}$, where n denotes the number of energy quanta in the CPW resonator, while e and g denote, respectively, the excited and the ground state of the superconducting qubit. Therefore, the corresponding Hilbert space, on which the Hamiltonian $H_{\rm cir}$ in Eq. (1) acts, can be written as the direct sum

$$V = \{|0,g\rangle\} \bigoplus_{n=0} V_n,$$

where the ground state (of the combination of the qubit and the CPW resonator) does not belong to any invariant subspace.

The basis of each subspace V_n can be transformed by rotating an angle

$$\theta_n = \frac{1}{2}\tan^{-1}\left(\frac{\eta\sqrt{n+1}}{\omega_q - \omega_0/2}\right) \tag{4}$$

such that the circuit Hamiltonian $H_{\rm cir}$ is diagonalized in the invariant subspace V_n with eigenvalues

$$E_n = \left(n+\frac{1}{2}\right)\omega_0 \pm \sqrt{\left(\omega_q - \frac{\omega_0}{2}\right)^2 + \eta^2(n+1)}\,, \tag{5}$$

where the second term constitutes the Rabi splitting for each energy level n. Written in the transformed basis

$$|\mu_n\rangle = \cos\theta_n\,|n,e\rangle - \sin\theta_n\,|n+1,g\rangle, \tag{6}$$

$$|\nu_n\rangle = \sin\theta_n\,|n,e\rangle + \cos\theta_n\,|n+1,g\rangle \tag{7}$$

and by neglecting the ground state $|0,g\rangle$, the circuit Hamiltonian (1) can be expressed in its diagonal "dressed" form as

$$H_{\rm cir} = \sum_n \left[E_n^{\mu}\,|\mu_n\rangle\,\langle\mu_n| + E_n^{\nu}\,|\nu_n\rangle\,\langle\nu_n|\right], \tag{8}$$

where E_n^{μ} (E_n^{ν}), associated with the basis vector $|\mu_n\rangle$ ($|\nu_n\rangle$), corresponds to the plus (minus) sign of the eigenvalue of Eq. (5) at the nth Rabi splitting. The corresponding dressed eigenvectors are diagrammatically illustrated as the lower (upper) lines on the right side of Fig. 2.

Note from Eq. (5) that the parameter ω_q provides a means to tune the level spacing of the superconducting qubits, through externally controlling gate voltages, or magnetic flux, or current [16–19]. Thus the dressed qubit can exhibit different responses to the probe field signal.

IV. COMPLEX SUSCEPTIBILITY

A. Three-level system

Originally, the undressed qubit has two levels. When this two-level system is coupled to a driving CPW resonator, the interaction "dresses" the system to have an infinite number of states, instead of two. These states are shown in Eqs. (6) and (7). The multilevel structure of the dressed system gives vast selections of three-level structures on which the EIT or the EIA effect can be demonstrated. Before we select three specific levels for our purpose, we shall rewrite the external part $H_{\rm ext}$ of the total Hamiltonian, which we have not discussed so far, in the transformed or dressed basis.

The transformed basis spans the product space of the qubit space and the resonator space. Considering this, we write the flip-up operator $\sigma_+ = I \otimes |e\rangle\langle g| = \sum_n |n,e\rangle\langle n,g|$ as the tensor product of two space bases in $H_{\rm ext}$. Taking the inner products of these basis vectors and those of the transformed basis, we find that, except for the first off-diagonal elements (i.e., $\langle\mu_{n+1}|\sigma_+|\mu_n\rangle$, $\langle\nu_{n+1}|\sigma_+|\nu_n\rangle$, $\langle\mu_{n+1}|\sigma_+|\nu_n\rangle$, and $\langle\nu_{n+1}|\sigma_+|\mu_n\rangle$), all the entries (including the diagonal ones) of the operator σ_+ in the new matrix representation are zero. The θ_n-dependent nonzero matrix elements are all real and, by using Eqs. (6) and (7), the new representation reads

$$\begin{aligned}\sigma_+ = \sum_n \{&-\cos\theta_{n+1}\sin\theta_n|\mu_{n+1}\rangle\langle\mu_n| + \sin\theta_{n+1}\cos\theta_n \\ &\times|\nu_{n+1}\rangle\langle\nu_n| - \sin\theta_{n+1}\sin\theta_n|\nu_{n+1}\rangle\langle\mu_n| \\ &+ \cos\theta_{n+1}\cos\theta_n|\mu_{n+1}\rangle\langle\nu_n|\}.\end{aligned} \tag{9}$$

This derivation applies equally well to the adjoint σ_-.

From Eq. (9), we see that the excitations of the qubit engage the nearest set of neighboring levels of the CPW resonator in a way that the transition coefficients depend on the device parameters of the superconducting qubit. Therefore, from the point of view of these dressed qubit levels, the process of energy pumping into a resonator through a mediating qubit [29] is a laddering of consecutive level jumps to the next $(n+1)$ dressed level.

Substituting Eq. (9) and its adjoint into Eq. (2), and also using Eq. (8), one reaches a total Hamiltonian expressed completely in the dressed basis. By selecting the three levels with lowest eigenenergies according to Eq. (5), that is,

$$\{|\mu_0\rangle, |\nu_0\rangle, |\mu_1\rangle\},$$

a Hamiltonian resembling that of a three-level atom with two associated dipole-field interactions is obtained:

$$\begin{aligned}H_\Lambda = {}& E_0^{\mu}\,|\mu_0\rangle\,\langle\mu_0| + E_0^{\nu}\,|\nu_0\rangle\,\langle\nu_0| + E_1^{\mu}\,|\mu_1\rangle\,\langle\mu_1| \\ &- \Omega_{\rm p}e^{-i\omega_{\rm p}t}\cos\theta_1\sin\theta_0\,|\mu_1\rangle\,\langle\mu_0| \\ &+ \Omega_{\rm c}e^{-i\omega_{\rm c}t}\cos\theta_1\cos\theta_0\,|\mu_1\rangle\,\langle\nu_0| + \text{H.c.}\end{aligned} \tag{10}$$

The three selected levels, whose transitions are coupled to the classical probe field of frequency $\omega_{\rm p}$ and the control field of frequency $\omega_{\rm c}$, are shown on the right side of the level diagram in Fig. 2. Note that when selecting the levels, the state $|0,g\rangle$, which did not participate in the basis transformation, is ignored. The selected states ($|\mu_0\rangle$, $|\nu_0\rangle$, and $|\mu_1\rangle$) correspond to the dressed ground state, metastable state, and excited state, respectively. Each of the classical fields, $\omega_{\rm p}$ and $\omega_{\rm c}$, can drive (i) transitions between the ground, metastable, and excited states, as well as (ii) those between levels of higher energies. We choose the frequencies of the classical fields such that the probe field $\omega_{\rm p}$ (the control field ω_c) is near resonant with the transition $|\mu_1\rangle\langle\mu_0|$ ($|\mu_1\rangle\langle\nu_0|$) for our discussion of the electromagnetically induced transparency and absorption effect. The two frequencies $\omega_{\rm p}$ and $\omega_{\rm c}$ can be considered to be far detuned from each other and from other transitions (including transitions to higher energy levels). Therefore, all other types of interactions can be neglected in the Hamiltonian (10).

B. Qubit-resonator interaction

The coupling coefficients of the three-level system, given in Eq. (10), depend not only on the Rabi frequencies $\Omega_{\rm p}$ and $\Omega_{\rm c}$ but also on the rotation angles θ_0 and θ_1. That is, the diagonalizing transformation partially determines the magnitude of the probe and control field couplings.

From Eq. (4), we observe that the diagonalizing angles at two different CPW-resonator levels obey the general relation

$$\frac{\tan 2\theta_n}{\tan 2\theta_m} = \frac{\sqrt{n+1}}{\sqrt{m+1}}.$$

If the levels are such that $m < n$, then $\theta_n > \theta_m$ in the first quadrant. Applying this relation to $m = 0$ and $n = 1$, we find

$$\theta_1 = \tfrac{1}{2}\tan^{-1}(\sqrt{2}\tan 2\theta_0),$$

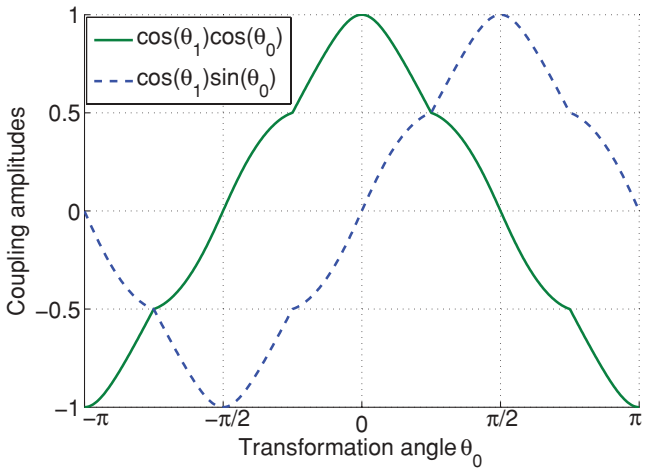

FIG. 3. (Color online) Coupling amplitudes of the dressed qubit to the probe field (denoted by the dashed curve) and to the control field (denoted by the solid curve).

which is not an everywhere-differentiable function with respect to θ_0. There exist nondifferentiable points at $(l\pi/2 + \pi/4)$, for integer l. Figure 3 plots the rotation-angle-dependent factors $(\cos\theta_1 \sin\theta_0)$ and $(\cos\theta_1 \cos\theta_0)$ in the coupling coefficients of Eq. (10), as functions of θ_0, over one period, within which four nonsmooth turning points can be spotted for each function.

From the first quadrant $(0 \leqslant \theta_0 \leqslant \pi/2)$ of Fig. 3, we note that the coupling amplitude between the dressed qubit and the probe field is monotonically increasing while that of the control field is monotonically decreasing. The two coupling amplitudes coincide at $\theta_0 = \pi/4$. Therefore, the rotation angle can be tuned in such a way that the coupling strengths between the dressed qubit and the external signals vary considerably, from $\theta_0 = 0$, where the coupling to the control field is maximized, to the opposite limit $\theta_0 = \pi/2$, where the coupling to the probe field is maximized.

Coherent trapping, usually discussed in the context of quantum optics, also occurs here in this superconducting dressed two-level system. If the initial state of the dressed qubit is prepared with equal populations in the two lower states with no phase difference [i.e., $|\psi(0)\rangle = (|\mu_0\rangle + |\nu_0\rangle)/\sqrt{2}$], then the interactions with the external signals, as described in Eq. (10), will drive the population at the excited level to be dependent only on the coupling Rabi frequencies Ω_p and Ω_c. In the dressed system, when the qubit level spacing reaches the exact values

$$\omega_q = \frac{\omega_0}{2} + \frac{\eta}{\tan[2\tan^{-1}(\Omega_c/\Omega_p)]},$$

the population at the upper lever will remain zero, while those of the two lower levels stay the same over all time t. The phenomenon of "trapping" is then achieved in the sense that the dressed system will remain in such a configuration with no population in the upper excited level, even though the classical signals are continually pumped into the system.

C. Demonstrating EIT via the complex susceptibility

Using the standard density matrix formalism [32], in this section, we demonstrate the EIT effect through the derivation of the first-order susceptibility of the dressed qubit. The dressed qubit acts as a signal-absorbing medium driven by the two external signals ω_p and ω_c, as schematically shown in Fig. 2, similar to the three-level atom with the optical fields given in Fig. 1(g). We will use the matrix element notation $\rho_{\alpha\beta} = |\alpha\rangle\langle\beta|$, where α and β can be one of the symbols μ,ν for the lower levels $|\mu_0\rangle,|\nu_0\rangle$ and 1 for the excited level $|\mu_1\rangle$; $\rho_{\alpha\beta}$ denotes level populations when $\alpha = \beta$, or transition amplitudes otherwise. We shall also use the following shorthand for the coupling coefficients:

$$\zeta_p(t) = -\Omega_p e^{-i\omega_p t}\cos\theta_1 \sin\theta_0,$$
$$\zeta_c(t) = \Omega_c e^{-i\omega_c t}\cos\theta_1 \cos\theta_0.$$

The matrix elements thence evolves according to Schroedinger's equation with respect to the Hamiltonian in Eq. (10), analogous to the optical Bloch equations,

$$\dot{\rho}_{\mu\mu} = -\Gamma_\mu \rho_{\mu\mu} - i\zeta_p \rho_{1\mu} + i\zeta_p^* \rho_{\mu 1}, \tag{11a}$$
$$\dot{\rho}_{\nu\nu} = -\Gamma_\nu \rho_{\nu\nu} - i\zeta_c \rho_{1\nu} + i\zeta_c^* \rho_{\nu 1}, \tag{11b}$$
$$\dot{\rho}_{11} = -\Gamma_1 \rho_{11} + i\zeta_p \rho_{1\mu} + i\zeta_c \rho_{1\nu} - i\zeta_p^* \rho_{\mu 1} - i\zeta_c^* \rho_{\nu 1}, \tag{11c}$$
$$\dot{\rho}_{\mu 1} = -\left[i\left(E_0^\mu - E_1^\mu\right) + \gamma_{\mu 1}\right]\rho_{\mu 1} - i\zeta_p(\rho_{11} - \rho_{\mu\mu}) + i\zeta_c \rho_{\mu\nu}, \tag{11d}$$
$$\dot{\rho}_{\nu 1} = -\left[i\left(E_0^\nu - E_1^\mu\right) + \gamma_{\nu 1}\right]\rho_{\nu 1} - i\zeta_c(\rho_{11} - \rho_{\nu\nu}) + i\zeta_p \rho_{\mu\nu}^*, \tag{11e}$$
$$\dot{\rho}_{\mu\nu} = -\left[i\left(E_0^\mu - E_0^\nu\right) + \gamma_{\mu\nu}\right]\rho_{\mu\nu} - i\zeta_p \rho_{\nu 1}^* + i\zeta_c^* \rho_{\mu 1}. \tag{11f}$$

In these equations, we have added phenomenologically the relaxation rate Γ_μ (Γ_ν,Γ_1) for the level $|\mu_0\rangle$ $(|\nu_0\rangle,|\mu_1\rangle)$ as well as the dephasing rate $\gamma_{\mu 1}$ $(\gamma_{\nu 1},\gamma_{\mu\nu})$ for the transition $|\mu_0\rangle\langle\mu_1|$ $(|\nu_0\rangle\langle\mu_1|,|\mu_0\rangle\langle\nu_0|)$. Note that the subscripts μ, ν, and 1 here refer to the levels $|\mu_0\rangle$, $|\nu_0\rangle$, and $|\mu_1\rangle$, respectively, to simplify the notation. This system of equations is homogeneous, which gives a zero steady-state solution (i.e., the system's thermal equilibrium state) when the coefficient matrix is nondegenerate. Therefore, we can assign, without loss of generality, the population under consideration entirely to the ground state, (i.e. $\rho_{\mu\mu}^{(0)} = 1$ and $\rho_{\nu\nu}^{(0)} = \rho_{11}^{(0)} = 0$) and the polarization $\langle \mathbf{P}^{(0)}\rangle$ (dipole moment) among the three energy levels at the zeroth-order expansion to zero value (i.e., $\rho_{\mu 1}^{(0)} = \rho_{\nu 1}^{(0)} = \rho_{\mu\nu}^{(0)} = 0$).

Since we are concerned with the dispersion and absorption spectrum of the dressed qubit, only the first-order perturbative expansion of the density matrix elements in Eqs. (11d)–(11f) are needed. Substituting the steady-state solution into these two equations and removing the time dependencies of the coefficients in the rotating frame of reference, $\rho_{\mu 1}^{(1)} \to \rho_{\mu 1}^{(1)} \exp\{-i\omega_p t\}$, $\rho_{\mu\nu}^{(1)} \to \rho_{\mu\nu}^{(1)} \exp\{-i(\omega_p + E_0^\nu - E_1^\mu)\}$, we have

$$\dot{\rho}_{\mu 1}^{(1)} = -(i\Delta + \gamma_{\mu 1})\rho_{\mu 1}^{(1)} + i\Omega_c \cos\theta_1 \cos\theta_0 \rho_{\mu\nu}^{(1)} - i\Omega_p \cos\theta_1 \sin\theta_0, \tag{12}$$

$$\dot{\rho}_{\mu\nu}^{(1)} = -(i\Delta + \gamma_{\mu\nu})\rho_{\mu\nu}^{(1)} + i\Omega_c \cos\theta_1 \cos\theta_0 \rho_{\mu 1}^{(1)}, \tag{13}$$

where

$$\Delta = \left(E_1^{\mu} - E_0^{\mu}\right) - \omega_{\mathrm{p}}$$

is the detuning between the probe field and the level spacing of the ground state and the excited state. The control field frequency ω_{c} is assumed to match the level spacing between the metastable state $|\nu_0\rangle$ and the excited state $|\mu_1\rangle$: $\omega_{\mathrm{c}} = E_1^{\mu} - E_0^{\nu}$.

The strength of the probe field is related to the polarization of the medium through the relation

$$\epsilon_0 \chi^{(1)} \Omega_{\mathrm{p}} = |\mathbf{d}_{\mu 1}|^2 \rho_{\mu 1},$$

where ϵ_0 denotes the vacuum permittivity and $\mathbf{d}_{\mu 1}$ the qubit dipole moment. Combining this relation with Eqs. (12) and (13) in steady state, we can find the first-order susceptibility

$$\chi^{(1)} = \chi' + i\chi''$$

decomposed into a real part

$$\chi' = Z\Delta[\Delta^2 - \gamma_{\mu 1}\gamma_{\mu\nu} - (\Omega_{\mathrm{c}} \cos\theta_1 \cos\theta_0)^2 + \gamma_{\mu\nu}(\gamma_{\mu 1} + \gamma_{\mu\nu})] \tag{14}$$

and an imaginary part

$$\chi'' = Z\left[\gamma_{\mu 1}\Delta^2 + \gamma_{\mu 1}\gamma_{\mu\nu}^2 + \gamma_{\mu\nu}(\Omega_{\mathrm{c}} \cos\theta_1 \cos\theta_0)^2\right], \tag{15}$$

where the common factor is

$$Z = \frac{|\mathbf{d}_{\mu 1}|^2}{\epsilon_0} \cos\theta_1 \sin\theta_0 \{\Delta^2(\gamma_{\mu 1} + \gamma_{\mu\nu})^2 + [\Delta^2 - \gamma_{\mu 1}\gamma_{\mu\nu} - (\Omega_{\mathrm{c}} \cos\theta_1 \cos\theta_0)^2]^2\}^{-1}.$$

Note that the dependencies of Eqs. (14) and (15) on the detuning Δ are similar to those of the susceptibilities of regular three-level atomic systems. The difference here is the extra dependence on the qubit level spacing ω_q through the transformation angles θ_1 and θ_0. First, the Rabi frequency $(\Omega_{\mathrm{c}} \cos\theta_1 \cos\theta_0)$, which describes the coupling strength of the control signal to the dressed qubit, has an explicit dependence on the angles θ_1 and θ_0. Second, the relaxation rates $\gamma_{\mu 1}$ and $\gamma_{\mu\nu}$ have implicit dependencies on these angles. These cosinusoidal dependencies will vary the magnitude of every term and will hence vary the functional behaviors of the two parts χ' and χ'' of the susceptibility. In the following sections, we will see that these dependencies are crucial to the tunability of the dressed qubit to become either transparent or absorptive.

V. DECAY RATES BETWEEN THE DRESSED LEVELS

A. Overview of recent theories

In this section, we study how the relaxation rates $\gamma_{\mu 1}$ and $\gamma_{\mu\nu}$ in Eqs. (14) and (15) and other dephasing rates are implicitly dependent on the qubit level spacing ω_q and other system parameters. In particular, we will determine how these decay rates are affected by the dressing process (i.e., after the qubit levels are rotated into the new dressed basis).

The decay of an undressed qubit induced by an environmental coupling has been extensively studied in Refs. [33] and [34] through a first-order perturbation model based on Bloch and Redfield's analysis [35] on what was called a relaxation or distribution matrix. The relaxation process induced by the environment has many implications on multilevel systems, including the lasing action of superconducting circuits [36].

The recent article by Wilson *et al.* [37] is the first study that took a step further to deal with the dressing effect on relaxation and dephasing, in which the resonator field couples to the z direction of the qubit and diagonalizing in a displaced basis results in a splitting of levels that has a Bessel-function dependence on the quantum number n. The approach here with the rotating wave approximation, in contrast, has a linear dependence of the splitting on n [cf. Eq. (5)]. This number n determines both the thermal distribution of energy quanta in the CPW resonator and the rotation angles of the levels in each invariant subspace, for which we expect to see a two-fold dependence of the relaxation rates on the level n. Moreover, the environmental temperature T determines the CPW resonator's thermal distribution, as well as the magnitude of the fluctuations induced by the thermal coupling of the nondressed qubit. Therefore, the dressed qubit has a two-fold dependence on the temperature T.

We will study each aspect of this dependence separately in the following sections. The direct fluctuations introduced by the thermal coupling before the dressing process will be discussed first. The indirect dependence through the resonator's thermal distribution after the dressing process will follow, where the implicit dependence on the qubit level spacing ω_q is also introduced.

B. Relaxation and dephasing before dressing

The two steps of computing the dressed decay rates can be separated by first assuming that the system has reached thermal equilibrium and the two-level qubit provides the only source of noise (i.e., the resonator has no thermal fluctuations). Following the standard methodology (e.g., in Ref. [33]), we describe the thermal environment by a single quantum variable X, which interacts with the qubit along all three directions through the Hamiltonian $H_I = (c_x\sigma_x + c_y\sigma_y + c_z\sigma_z)X$. Among the interaction coefficients, those of the σ_x and σ_y directions affect the population decay between two levels, that is, they contribute a total relaxation rate

$$r_1 = r_\downarrow + r_\uparrow,$$

which consists of a "down" relaxation rate $r_\downarrow$ and an "up" relaxation rate $r_\uparrow$:

$$r_\downarrow = |c_x + ic_y|^2 S_X(\omega)/4,$$
$$r_\uparrow = |c_x + ic_y|^2 S_X(-\omega)/4.$$

The S_X shown in these expressions indicate the power spectrum of the heat bath; its value has an exponential dependence on the environment temperature T:

$$S_X(\omega) = \frac{1}{2\pi}\int_{-\infty}^{\infty} \mathrm{d}\omega' \langle X(\omega)X(\omega')\rangle = \frac{R\omega}{2\pi} \coth\left(\frac{\omega}{2k_B T}\right),$$

where R denotes a nominal resistance.

The σ_z direction of the interaction coefficients contributes a part, r_φ, of the total dephasing rate, which is known as the

pure dephasing part:

$$r_\varphi = |c_z|^2 S_X(0)/2.$$

The interactions along σ_x and σ_y directions contribute the other part, r_1, of the dephasing, which make the total dephasing rate of the qubit sum to

$$r_2 = \frac{r_1}{2} + r_\varphi.$$

C. Relaxation and dephasing after dressing

Given the level mixings due to the unitary transformations in Eqs. (6) and (7), the fluctuations of the dressed levels become the superpositions of the fluctuations originated from the states of the undressed qubit.

The density matrix element for the lowest level of the dressed qubit, expanded in the undressed basis, reads

$$|\mu_0\rangle\langle\mu_0| = \cos^2\theta_0|0,e\rangle\langle 0,e| + \sin^2\theta_0|1,g\rangle\langle 1,g| - \cos\theta_0\sin\theta_0[|0,e\rangle\langle 1,g| + \text{H.c.}].$$

We see that this matrix element has the diagonal parts and the off-diagonal parts in the undressed basis. To simplify the formulation, we assume that the dressed qubit has reached thermal equilibrium and ignore the system relaxation due to the energy exchange between the CPW resonator and the qubit, that is, the off-diagonal parts. Then by tracing out the subspace of the resonator part by assuming its energy quanta has a Boltzmann distribution, we can obtain the reduced density matrix element

$$\rho'_{\mu\mu} = (1 - e^{-\beta\omega_0})[\cos^2\theta_0|e\rangle\langle e| + e^{-\beta\omega_0}\sin^2\theta_0|g\rangle\langle g|],$$

where $\beta = 1/k_B T$ denotes the inverse temperature. Considering that the two levels of the undressed qubit contribute equally to the up and down relaxations, we arrive at the relaxation rate Γ_μ of the lowest energy level $|\mu_0\rangle$ of the dressed qubit,

$$\Gamma_\mu = \frac{|c_x + ic_y|^2 S_X(\omega)}{4}(1 - e^{-\beta\omega_0})[\cos^2\theta_0 + e^{-\beta\omega_0}\sin^2\theta_0]. \tag{16a}$$

Using similar steps, we can derive the relaxation rates (Γ_ν and Γ_1) of the other energy levels ($|\nu_0\rangle$ and $|\mu_1\rangle$) as well as their dephasing rates ($\gamma_{\mu 1}$, $\gamma_{\nu 1}$, and $\gamma_{\mu\nu}$):

$$\Gamma_\nu = \frac{|c_x + ic_y|^2 S_X(\omega)}{4}(1 - e^{-\beta\omega_0})[\sin^2\theta_0 + e^{-\beta\omega_0}\cos^2\theta_0], \tag{16b}$$

$$\Gamma_1 = \frac{|c_x + ic_y|^2 S_X(\omega)}{4}e^{-\beta\omega_0}(1 - e^{-\beta\omega_0}) \times [\cos^2\theta_1 + e^{-\beta\omega_0}\sin^2\theta_1], \tag{16c}$$

$$\gamma_{\mu 1} = -\frac{|c_z|^2 S_X(0)}{2}e^{-\beta\omega_0}(1 - e^{-\beta\omega_0})\sin\theta_0\cos\theta_1, \tag{16d}$$

$$\gamma_{\nu 1} = \frac{|c_z|^2 S_X(0)}{2}e^{-\beta\omega_0}(1 - e^{-\beta\omega_0})\cos\theta_0\cos\theta_1, \tag{16e}$$

$$\gamma_{\mu\nu} = \frac{|c_x + ic_y|^2 S_X(\omega)}{4}(1 - e^{-\beta\omega_0})^2\cos\theta_0\sin\theta_0. \tag{16f}$$

We note from Eq. (16f) that the dephasing rate $\gamma_{\mu\nu}$ between the split states $|\mu_0\rangle$ and $|\nu_0\rangle$, which share the same number of energy quanta, originates from the relaxation rates of the undressed qubit levels $|e\rangle$ and $|g\rangle$. Therefore, in transforming the basis for diagonalization, the roles of relaxation and dephasing have exchanged.

The total relaxation rate among the three dressed levels becomes now

$$\Gamma = \Gamma_\mu + \Gamma_\nu + \Gamma_1,$$

which has a two-fold dependence on the environment temperature T: through the noise spectrum $S_X(\omega)$ and through the resonator distribution $\exp(-\beta\omega_0)$. The total relaxation rate Γ is also tunable by the qubit level spacing ω_q through the transformation angle θ_0.

VI. TUNING THE ELECTROMAGNETICALLY INDUCED TRANSPARENCY AND ABSORPTION

A. Local extrema of the susceptibility

The qubit, together with the CPW resonator, acts as a nonlinear medium of electron propagation in the quantum circuit. This nonlinear medium gives the rotation-angle-dependent and relaxation-rate-dependent responses of both the dispersion and the absorption to the incident probe signal $\Omega_p e^{-i\omega_p t}$. These two responses are quantified by the real and the imaginary parts of the susceptibility, respectively, in Eqs. (14) and (15). Since the relaxation rates $\gamma_{\mu 1}, \gamma_{\mu\nu}$ themselves depend on the rotation angles θ_0, θ_1 [cf. Eqs. (16d)–(16f)], which in turn depend on the qubit level spacing ω_q [cf. Eq. (4)], the spacing ω_q tunes the dispersion and absorption spectra by controlling the Josephson coupling energy.

The absorption spectrum as a function of the detuning Δ between the probe signal and the dressed level spacing $(E_0^\mu - E_1^\mu)$ is particularly interesting with its number of maxima depending on the spacing ω_q. The derivative of χ'' with respect to Δ is the product of Δ and a quartic expression of Δ. Therefore, the absorption spectrum always takes an extremal value at the zero root $\Delta_0 = 0$. The quartic expression is actually biquadratic, whose two roots are given by

$$\Delta_\pm = \pm\frac{1}{\sqrt{\gamma_{\mu 1}}}\{-\gamma_{\mu\nu}[\zeta_c^2(0) + \gamma_{\mu 1}\gamma_{\mu\nu}] + (\gamma_{\mu 1} + \gamma_{\mu\nu})\zeta_c(0)\sqrt{\zeta_c^2(0) + \gamma_{\mu 1}\gamma_{\mu\nu}}\}^{1/2}, \tag{17}$$

where the other two roots that are associated with the negative sign of the second term are omitted since the detuning Δ can only admit real values. The two admissible roots coincide and meet the zero root (i.e., $\Delta_\pm = \Delta_0 = 0$) when

$$(\Omega_c\cos\theta_1\cos\theta_0)^2 + \gamma_{\mu 1}\gamma_{\mu\nu} = 0. \tag{18}$$

That is, at near resonance $\omega_q \approx \omega_0/2$, when the qubit level spacing reaches the critical values

$$\lambda_{C,\pm} = \frac{1}{2}\left\{\omega_0 \pm \frac{\eta}{F^2 - \sqrt{2}}[(\sqrt{2}+1)F^2 + 2\sqrt{2} - F\sqrt{(\sqrt{2}-1)^2F^2 + 16 + 8\sqrt{2}}]\right\}, \tag{19}$$

where

$$F(\Omega_c,T)=\frac{8\Omega_c^2 e^{\beta\omega_0}(1-e^{-\beta\omega_0})^{-3}}{|c_x+ic_y|^2|c_z|^2S_X(0)S_X(\omega)}$$

is a control field amplitude-dependent and temperature-dependent factor. We can also check that the condition $(\Omega_c\cos\theta_1\cos\theta_0)^2+\gamma_{\mu1}\gamma_{\mu\nu}>0$ has already guaranteed the right-hand side of Eq. (17) to be greater than zero (see the Appendix).

Consequently, inside the critical range $\lambda_{C,-}<\omega_q<\lambda_{C,+}$, the only admissible root of $d\chi''/d\Delta$ occurs at the zero point, and from the second-order derivative, it can be seen that this root corresponds to a local maximum. In the opposite case, when the qubit level spacing ω_q is tuned outside the critical range, two new extrema arise in the absorption spectrum, giving a total of three turning points in the absorption curve. Because χ'' is an even function of Δ, the original peak point at zero detuning splits symmetrically about the origin, creating two symmetric peaks whose distance $(\Delta_+-\Delta_-)$ is extended when ω_q is tuned away from the critical values $\lambda_{C,\pm}$ at either end, whereas the original peak

$$\chi''|_{\Delta_0}\propto\left[1+\Omega_c^2\frac{\cos\theta_1\cos\theta_0}{C\sin^2\theta_0}\right]^{-1}$$

itself, where C denotes some constant, starts to dip from a maximum value to a local minimum. This local minimum tends to zero when the spacing ω_q is tuned away from its resonant value $\omega_0/2$ and the amplitude Ω_c of the control field is increased.

This "peaking-to-dipping" transition (or the increase of the number of extrema) indicates the *switching of the dressed qubit from being transparent to being absorptive* to the probe field. The magnitude of the qubit level spacing ω_q with respect to the frequency ω_0 of the resonator field determines the nature of the dressed medium. The critical condition of Eq. (18) indicates the competition between the population pumping to the excited level and the spontaneous relaxations to the ground state. The transparency effect is present only when the coherent pumping is sufficiently strong to overcome the relaxation; otherwise, the probe signal is trapped and the dressed medium becomes absorbing.

While the imaginary part of the susceptibility is an even function of Δ, the real part is odd and one order higher in Δ than the imaginary part. The dispersion spectrum similarly admits multiple local extrema, though the dispersion is always zero at $\Delta=0$ for any value of qubit level spacing ω_q because of the odd symmetry about the origin. However, when sweeping ω_q across the resonance point $\omega_0/2$, the spectrum is inverted (i.e. the dispersion is switched from positive to negative or vice versa).

B. Near degeneracy and the switching from closed to open transitions

The phenomena discussed in the last section are somewhat analogous to those presented in Refs. [12,13], so here we give a physical interpretation of the tuning from transparency to absorption using the terminology of atomic physics.

The three dressed states $|\mu_0\rangle$, $|\nu_0\rangle$, and $|\mu_1\rangle$ that we have selected as the basis of the three-level system have tunable level spacings based on the transformation angles θ_0 and θ_1, which are defined by the detuning between the parameters ω_q and ω_0. After coupling to the strong control field, the two dressed states $|\nu_0\rangle$ and $|\mu_1\rangle$ will have line broadening. The metastable state $|\nu_0\rangle$ in particular might be so broadened that it overlaps with the ground state $|\mu_0\rangle$. Such a case most easily occurs at resonance with $\omega_q=\omega_0/2$, where the spacing between the lower two states $|\mu_0\rangle$ and $|\nu_0\rangle$ is minimized to 2η [cf. Eq. (5)].

When the overlap occurs, the three-level system becomes effectively a two-level system. The lower two levels $|\mu_0\rangle$ and $|\nu_0\rangle$ become quasidegenerate or near degenerate; more precisely, they degenerate into a single ground state and differ from each other only as hyperfine levels of the common ground state. The minimal amplitude Ω_c of the coupling needed for overlapping can be roughly estimated by using a first-order perturbative expansion. Considering the spacing between the metastable state $|\nu_0\rangle$ and the excited state $|\mu_1\rangle$ to be $E_1^\mu-E_0^\nu=\omega_0-(\sqrt{2}+1)\eta$, we find the level shift of $|\nu_0\rangle$ up to first order to be

$$E_0^{\nu(1)}-E_0^{\nu(0)}=\frac{|\Omega_c|^2}{\omega_0-(\sqrt{2}+1)\eta}.$$

After equating this to 2η, the amplitude needed can be obtained as

$$\Omega_c=\sqrt{2\eta[\omega_0-(\sqrt{2}+1)\eta]}. \tag{20}$$

Comparing Eq. (20) with Eq. (18), we can observe that, in order to exhibit electromagnetically induced transparency, the coupling amplitude Ω_c would have to be within a range such that it can simultaneously overcome the spontaneous relaxation and yet prevent the system from being degenerate, in addition to the requirement that ω_q be outside the critical range indicated by Eq. (19). Without this range, the dressed medium becomes unresponsive to the incident probe signal and the absorption spectrum becomes flat.

If we draw the analogy of the lower dressed levels to the Zeeman sublevels of the degenerate ground state [12], then $|\mu_0\rangle$ and $|\nu_0\rangle$ can be deemed sharing the same nonzero "angular momentum." The remaining factor for deciding the dressed medium to be transparent or absorbing depends on whether the transition between the two sublevels is open or closed—in other words, whether the transitions within the three-level system are noncyclic (Λ type) or cyclic (Δ type). Different from the usual case, where this factor is determined by the hyperfine structure of a particular atom, the dressed qubit system we discuss here has this factor effectively determined by the dressed relaxation rates $\gamma_{\mu1}$ and $\gamma_{\mu\nu}$.

From Eqs. (16d)–(16f), we observe that unlike the usual multilevel SQUID systems, the relaxation rates of the dressed qubit are tunable through the transformation angles θ_0 and θ_1. In addition, the relaxation rate $\gamma_{\mu\nu}$ between the lower levels is actually derived from the dephasing rate r_φ of the undressed qubit. The type of transitions in the dressed qubit thus becomes exploitable since the dephasing rates of the superconducting qubits are in general much greater than their relaxation rates r_1 and the different dependencies on the transformation angles control whether $|\gamma_{\mu\nu}|>|\gamma_{\mu1}|$ or $|\gamma_{\mu\nu}|<|\gamma_{\mu1}|$.

When the qubit is closely resonant with the CPW resonator, or precisely, ω_q is within the critical range between $\lambda_{C,-}$ and $\lambda_{C,+}$, the magnitude of $\gamma_{\mu\nu}$ is greater, under which the flipping processes of the populations between the ground and the metastable states dominate over the excitation process from the ground state to the excited state. The transition between the ground and the metastable states is thus closed, effectively degenerating the two levels and making the three-level system operate in a Δ-type setting. On the other hand, when the qubit is off-resonant with the CPW resonator, the opposite condition $\gamma_{\mu 1} > \gamma_{\mu\nu}$ is met and the lower two levels become sufficiently nondegenerate that the transitions among the three levels cannot be considered cyclic. The system then operates in the usual Λ-type setting that electromagnetically induced transparency can take place.

VII. NUMERICAL ANALYSIS

We now study the two parts of the susceptibility by considering experimentally accessible parameters. We first examine the dressed charge qubit, which was experimentally realized in Refs. [23,37,38]. We give the variation of the susceptibility against multiple parameters and identify the effective ranges of the qubit level spacing for the EIT and EIA. The cases for phase and flux qubits are discussed later to show that the arguments for charge qubits can be applied to other qubits, for tuning the susceptibility to different operating regimes.

A. Charge qubit

Without loss of generality, we now assume that the resonator frequency is fixed at, for example, $\omega_0/2\pi = 7$ GHz. We consider the charge qubit model with the following parameters: The qubit has a junction energy $E_J/2\pi = 2.6$ GHz and a charge energy in the gigahertz range that we use to tune the qubit level spacing by varying the gate reduced charge number n_g; the coupling coefficient between them is assumed to be $\eta/2\pi = 100$ MHz. The undressed relaxation and dephasing times of the qubit are taken as $1/r_1 = 0.7\,\mu$s and $1/r_2 = 48$ ns, respectively. The operating temperature is assumed to be 20 mK.

Figure 4 plots both the real χ' and the imaginary χ'' parts of the susceptibility χ in normalized units as a function of the normalized probe-signal detuning Δ/Δ' (with respect to the normalizing constant $\Delta'/2\pi = 25$ MHz) and the normalized qubit level spacing ω_q/ω_q' (with respect to the normalizing constant $\omega_q'/2\pi = 3.5$ GHz) near the resonance range of the dressed qubit. The strongly coupled control field can achieve a coupling amplitude on the order of 10 MHz [23]; in the plot here a value of $\Omega_c/2\pi = 12$ MHz is assumed.

For the imaginary part χ'' (warm colored: red or yellow), we are able to observe the absorption peaking at the resonant frequency $\omega_q = \omega_0/2 = 2\pi \times 3.5$ GHz and its immediate falloff when ω_q is tuned slightly off resonance. Along with the attenuation of the magnitude is the symmetric splitting of the peak about the zero detuning point $\Delta = 0$ at either off-resonant side. The zero-detuning point itself falls from its maximum value to its local minimum along the path of off resonance, indicating the switching of the dressed medium

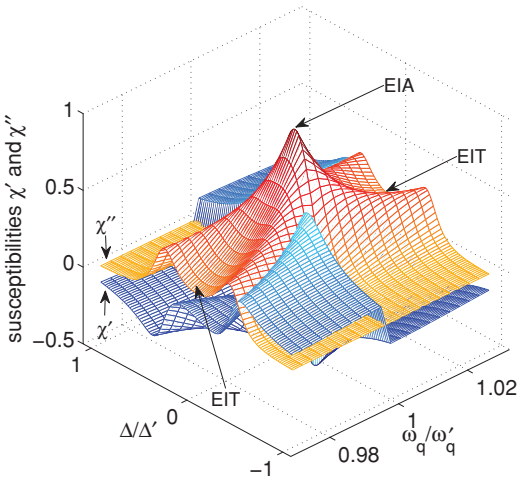

FIG. 4. (Color online) Real part χ' (blue) and imaginary part χ'' (red or yellow) of the normalized susceptibility of the dressed charge qubit versus the detuning Δ and the qubit level spacing ω_q. The detuning abscissa is normalized with respect to $\Delta'/2\pi = 25$ MHz; the qubit-level-spacing abscissa is normalized with respect to $\omega_q'/2\pi = 3.5$ GHz. This plot indicates the dispersion and absorption spectra of a probe signal over different operating ranges.

from "maximally absorbing" to being transparent to the probe signal.

The switching phenomenon is better illustrated in Fig. 5(a) where the imaginary part χ'' of the susceptibility is plotted for various values of the spacing ω_q. We note that the susceptibility obtains a maximum value and a minimum half-width with a Lorentzian shape when the dressed medium is resonant (the thickened curve for $\omega_q/2\pi = 3.5$ GHz). Following the detuning between the qubit and the CPW resonator, the half-width starts to spread out while the peak starts to dent. The switching occurs at the critical value $\lambda_C/2\pi = 3.40$ GHz, according to the approximate analytical solution of Eq. (19), where the qubit-to-resonator coupling η is not very large. A numerical estimate gives $\lambda_C/2\pi \approx 3.47$ GHz, as can be seen from Fig. 5(a).

The plot of Fig. 4 also shows that the falloff of the absorption is even symmetric about the resonance point $\omega_q = \omega_0/2$, becauset χ'' is an even function of the dressed relaxation rates $\gamma_{\mu 1}$ and $\gamma_{\mu\nu}$, which in turn are odd functions of the qubit spacing ω_q. This symmetry verifies the exchangeable roles of the near-degenerate levels $|\mu_0\rangle$ and $|\nu_0\rangle$: When $\omega_q < \omega_0/2$, $|\mu_0\rangle$ has the lower eigenenergy of the dressed states and is regarded as the ground state that couples to the probe signal, while $|\nu_0\rangle$ is regarded as the metastable state; when $\omega_q > \omega_0/2$, $|\mu_0\rangle$ becomes the metastable level and $|\nu_0\rangle$ becomes the ground state.

In Fig. 4, for the real part χ' (blue colored), we can see the dispersion spectrum having an odd symmetry around the zero probe detuning point $\Delta = 0$ [i.e. $\chi'(\omega_q)|_{\Delta=0} = 0$] throughout the range of the qubit spacing ω_q. Unlike χ'', this real part χ' of the susceptibility is an odd function of the dressed relaxation rates, resulting in its odd symmetry of ω_q around the resonance point $\omega_q = \omega_0/2$, which is better illustrated in Fig. 5(b). There, the dispersion spectrum for various values of ω_q is plotted versus the detuning Δ. The one curve at

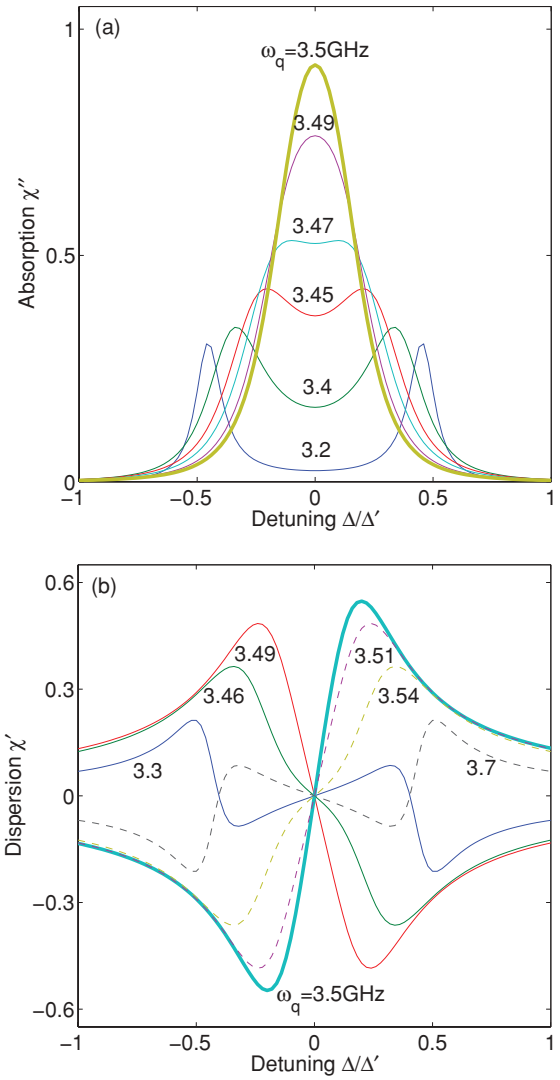

FIG. 5. (Color online) Normalized susceptibility spectra at typical values of the qubit level spacing ω_q plotted versus the scaled detuning Δ/Δ': (a) the absorption $\chi'' = \mathrm{Im}[\chi]$ and (b) the dispersion $\chi' = \mathrm{Re}[\chi]$. The curves that correspond to the resonant frequency $\omega_0/2 = 2\pi \times 3.5$ GHz are thickened and all the numbers indicate the value of ω_q taken (in unit of GHz) in both (a) and (b). Note that in (a) a dip appears at the center of the curve about $\omega_q/2\pi \approx 3.47$ GHz, which indicates the *switching of the dressed qubit from being absorptive* (>3.47 GHz) *to being transparent* (<3.47 GHz). In (b), the curves that correspond to ω_q below $\omega_0/2$ are solid and those above $\omega_0/2$ are dashed. Note that the solid and dashed curves with equal distance from the resonance $\omega_0/2$ are symmetric counterparts of each other. Their roles for positive and negative dispersion across the range of the detuning Δ are exchanged above and below the resonance frequency.

resonance ($\omega_q/2\pi = 3.5$ GHz) is thickened and the ones that have their symmetric counterparts below resonance are shown as dashed curves, from which we can observe the switching from positive dispersion to negative dispersion of the dressed medium discussed in Sec. VI.

In addition to the spacing ω_q, tuning the dressed qubit from transparency to absorption also depends on the dressed system's coupling strength Ω_c to the control field since this

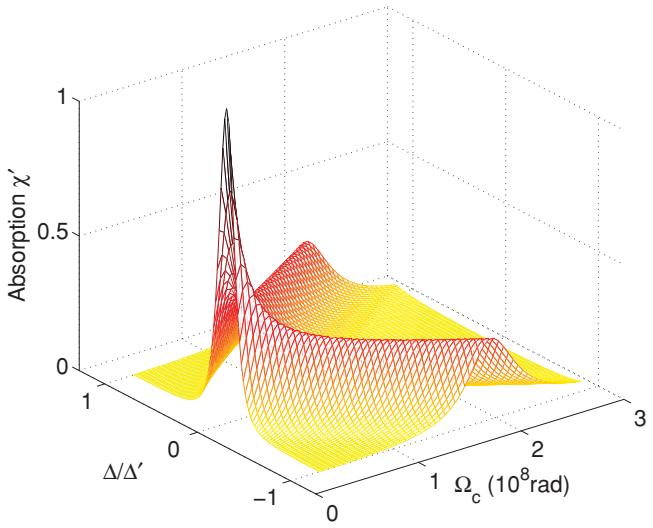

FIG. 6. (Color online) Plot of the normalized absorption spectrum $\chi'' = \mathrm{Im}[\chi]$ versus the normalized detuning Δ/Δ' and the coupling amplitude Ω_c to the control field.

coupling strength directly affects the absorption [cf. Eq. (15)]. Its influence is illustrated in Fig. 6 where the absorption is plotted against Δ/Δ' (over the same range as in Fig. 4) and Ω_c (from 4.5 to 45 MHz) while the qubit spacing is held at a typical value $\omega_q/2\pi = 3.4$ GHz. We can notice the single peaking at the lower end of the coupling to the control field, where the dressed medium is weakly driven by the control field and exhibits a population trapping of the probe signal. Toward higher values of the coupling, the excited state of the dressed three-level system is sufficiently detuned from the probe signal that it starts to exhibit the transparency effect. Then similar to ordinary Λ-type atoms, the dressed qubit has its twin absorption peaks further apart when the coupling strength is increased.

B. Phase qubits

We now examine our general theory of the tunable transparency and absorption effects on other superconducting quantum circuit systems.

For a phase qubit, we adopt the experimental parameters of Ref. [30]: The CPW resonator has a frequency $\omega_0/2\pi = 6.57$ GHz; the coupling strength between the resonator and the qubit is fixed at $\eta/2\pi = 19$ MHz; the undressed relaxation and dephasing times of the qubit are, respectively, 650 and 150 ns. The coupling strength to the control signal is assumed to be $\Omega_c/2\pi = 3.85$ MHz. The operation temperature is held at 25 mK. The normalized absorption spectrum is plotted as a contour plot versus the normalized qubit level spacing ω_q/ω_q' with respect to the charge qubit case (ω_q from 3.2 to 3.37 GHz; normalizing constant ω_q the same as that of the charge qubit) and the normalized probe detuning Δ/Δ' (Δ from -6.5 to 6.5 MHz; normalizing constant Δ' the same as that of the charge qubit) in Fig. 7(a).

Similar to the case of a charge qubit in the last section, the peak at the center of the contour falls off symmetrically as the qubit spacing is tuned off the resonant frequency $\omega_q/2\pi = 3.285$ GHz. The peak also splits symmetrically

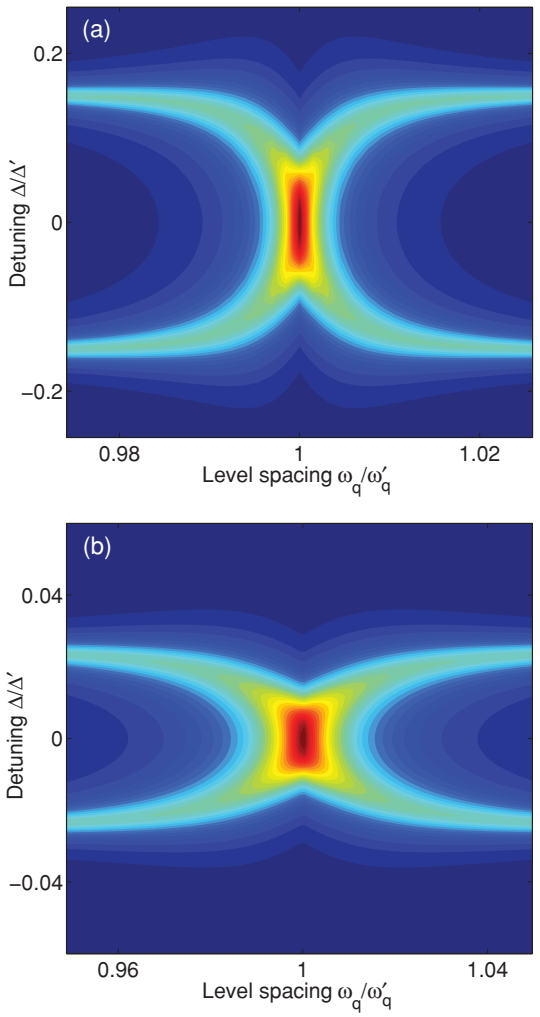

FIG. 7. (Color online) Contour plots of the normalized absorption spectra χ'' versus the normalized detuning Δ/Δ' on the vertical axis and the normalized qubit level spacing ω_q/ω'_q on the horizontal axis (a) for a phase qubit and (b) for a flux qubit. The red end of the color spectrum (i.e., the centers of both contour plots) indicates peak values of the absorption, where the qubit is maximally dressed with a rotation angle $\theta_0 = \pi/2$. The deep blue end of the color spectrum for $\Delta/\Delta' = 0$ (i.e., the middle sections of the left and right borders of both plots) indicates the minimum values of the absorption, where the qubit is dressed with a rotation angle $\theta_0 < \pi/2$. Namely, maximum transmission due to EIT occurs at those blue ends.

around the zero detuning $\Delta = 0$, and it enters from the absorption region into the transparency region at the critical frequency $\lambda_C/2\pi = 3.266$ GHz according to Eq. (19). The half-widths of the absorption peaks decrease along with the falloff of the magnitude.

C. Flux qubits

For a flux qubit, we adopt the experimental parameters of Ref. [31]: The CPW resonator has oscillating frequency $\omega_0/2\pi = 9.907$ GHz; the qubit-resonator coupling strength is $\eta/2\pi \approx 100$ MHz; the undressed relaxation and dephasing times of the qubit are, respectively, 1.9 and 1 μs [39]. The coupling strength to the control signal is set to $\Omega_c/2\pi = 0.63$ MHz. The operation temperature is 50 mK. The normalized absorption spectrum of the dressed flux qubit is also plotted as a contour plot versus the normalized qubit level spacing ω_q/ω'_q with respect to the charge qubit case (ω_q from 4.7 to 5.2 GHz; normalizing constant ω'_q the same as that of the charge qubit) and the normalized probe detuning Δ/Δ' (Δ from -1.5 to 1.5 MHz; normalizing constant Δ' the same as that of the charge qubit) in Fig. 7(b).

Similar operating regions of transparency and absorption can be observed in this flux qubit system compared to the other qubit systems discussed before, except for the scale of variations. For instance, comparing Figs. 7(a) and 7(b), we see that the falloff of the magnitude along the zero detuning is relatively slower in the flux qubit case due to the slower dephasing time of the undressed flux qubit. The switching occurs at the critical frequency $\lambda_C/2\pi = 4.854$ GHz. In this case, the absorption peaks also split out slower and have narrower half-widths.

VIII. CONCLUSION

We have proposed a method to realize the effects of both EIT and EIA on superconducting quantum circuits using dressed states derived from the coupling between an arbitrary type of two-level superconducting junction qubits and a coplanar waveguide resonator. The use of dressed states alleviates the need to maintain a multilevel structure of the Josephson devices and gives rise to tunable relaxation rates between the energy levels. The tunable structure of the levels leads to the switching between EIT and EIA, which depends on the variable qubit level spacing and is associated with the open or closed transition structure and the hyperfine degeneracy of the dressed three-level system.

Our investigation demonstrates another example of nonlinear optical phenomena implementable on superconducting quantum circuits. We can also see that the special characteristics of Josephson junction devices, the externally controllable Josephson coupling energy in this case, could bring new perspectives to the study of quantum optics where, for example, the many parameters are usually fixed for the particular type of atom studied and the cavity QED system that surrounds it. The switching between EIT and EIA might have important applications for the control of superconducting circuits and for quantum information transfer in these systems.

ACKNOWLEDGMENTS

We thank Prof. C. P. Sun for discussions. FN was supported in part by the National Security Agency, Laboratory of Physical Sciences, Army Research Office, National Science Foundation Grant No. 0726909, JSPS-RFBR Contract No. 09-02-92114, MEXT Kakenhi on Quantum Cybernetics, and FIRST (Funding Program for Innovative R&D on S&T). YXL acknowledges support from the National Natural Science Foundation of China under Grant No. 10975080.

APPENDIX: CONDITION OF LOCAL EXTREMA FOR THE SUSCEPTIBILITY

The two roots of Eq. (17) that correspond to local extrema of the dispersion spectrum must satisfy

$$(\gamma_{\mu 1}+\gamma_{\mu\nu})\zeta_c\sqrt{\zeta_c^2+\gamma_{\mu 1}\gamma_{\mu\nu}}-\gamma_{\mu\nu}\left(\zeta_c^2+\gamma_{\mu 1}\gamma_{\mu\nu}\right)>0,$$

which is equivalent to

$$(\gamma_{\mu 1}+\gamma_{\mu\nu})\zeta_c>\gamma_{\mu\nu}\sqrt{\zeta_c^2+\gamma_{\mu 1}\gamma_{\mu\nu}}.$$

When squaring the two sides, this inequality implies

$$\gamma_{\mu 1}^2\zeta_c^2+2\gamma_{\mu 1}\gamma_{\mu\nu}\zeta_c^2-\gamma_{\mu 1}\gamma_{\mu\nu}^3>0.$$

For $\zeta_c^2>-\gamma_{\mu 1}\gamma_{\mu\nu}$, with the relaxation rates taking values $\gamma_{\mu 1}<0$ and $\gamma_{\mu\nu}>0$ from Eqs. (16d)–(16f), we have

$$\begin{aligned}&\gamma_{\mu 1}\left\{(\gamma_{\mu 1}+2\gamma_{\mu\nu})\zeta_c^2-\gamma_{\mu\nu}^3\right\}\\&>\gamma_{\mu 1}\left\{-(\gamma_{\mu 1}+2\gamma_{\mu\nu})\gamma_{\mu 1}\gamma_{\mu\nu}-\gamma_{\mu\nu}^3\right\}\\&=-\gamma_{\mu 1}\gamma_{\mu\nu}(\gamma_{\mu 1}+\gamma_{\mu\nu})^2>0,\end{aligned}$$

so the real roots exist under this condition.

[1] S. E. Harris, J. E. Field, and A. Imamoglu, Phys. Rev. Lett. **64**, 1107 (1990); S. E. Harris, Phys. Today **50**, 36 (1997).

[2] M. Fleischhauer, A. Imamoglu, and J. P. Marangos, Rev. Mod. Phys. **77**, 633 (2005).

[3] C. L. G. Alzar, M. A. G. Martinez, and P. Nussenzveig, Am. J. Phys. **70**, 37 (2002).

[4] L. He, Y. X. Liu, S. Yi, C. P. Sun, and F. Nori, Phys. Rev. A **75**, 063818 (2007).

[5] X. Yuan, H. Goan, C. Lin, K. Zhu, and Y. Jiang, New J. Phys. **10**, 095016 (2008).

[6] R. S. Bennink, R. W. Boyd, C. R. Stroud Jr., and V. Wong, Phys. Rev. A **63**, 033804 (2001).

[7] K. V. R. M. Murali, Z. Dutton, W. D. Oliver, D. S. Crankshaw, and T. P. Orlando, Phys. Rev. Lett. **93**, 087003 (2004); Z. Dutton, K. V. R. M. Murali, W. D. Oliver, and T. P. Orlando, Phys. Rev. B **73**, 104516 (2006).

[8] M. A. Sillanpää, J. Li, K. Cicak, F. Altomare, J. I. Park, R. W. Simmonds, G. S. Paraoanu, and P. J. Hakonen, Phys. Rev. Lett. **103**, 193601 (2009).

[9] J. Q. You, Y. X. Liu, C. P. Sun, and F. Nori, Phys. Rev. B **75**, 104516 (2007).

[10] M. Müller, F. Homann, R.-H. Rinkleff, A. Wicht, and K. Danzmann, Phys. Rev. A **62**, 060501(R) (2000).

[11] S. Wielandy and A. L. Gaeta, Phys. Rev. A **58**, 2500 (1998).

[12] A. M. Akulshin, S. Barreiro, and A. Lezama, Phys. Rev. A **57**, 2996 (1998); A. Lezama, S. Barreiro, and A. M. Akulshin, *ibid.* **59**, 4732 (1999).

[13] C. Goren, A. D. Wilson-Gordon, M. Rosenbluh, and H. Friedmann, Phys. Rev. A **68**, 043818 (2003).

[14] Y. X. Liu, J. Q. You, L. F. Wei, C. P. Sun, and F. Nori, Phys. Rev. Lett. **95**, 087001 (2005).

[15] F. Deppe *et al.*, Nat. Phys. **4**, 686 (2008).

[16] Y. Makhlim, G. Schön, and A. Shnirman, Rev. Mod. Phys. **73**, 357 (2001).

[17] J. Q. You and F. Nori, Phys. Today **58**, 42 (2005).

[18] J. Clarke and F. K. Wilhelm, Nature (London) **453**, 1031 (2008).

[19] G. Wendin and V. S. Shumeiko, in *Handbook of Theoretical and Computational Nanotechnology*, edited by M. Rieth and W. Schommers (American Scientific Publishers, Los Angeles, 2006).

[20] R. J. Schoelkopf and S. M. Girvin, Nature (London) **451**, 664 (2008).

[21] Y. X. Liu, C. P. Sun, and F. Nori, Phys. Rev. A **74**, 052321 (2006).

[22] G. S. Agarwal, T. N. Dey, and S. Menon, Phys. Rev. A **64**, 053809 (2001).

[23] C. M. Wilson, T. Duty, F. Persson, M. Sandberg, G. Johansson, and P. Delsing, Phys. Rev. Lett. **98**, 257003 (2007).

[24] L. Zhou, Z. R. Gong, Y. X. Liu, C. P. Sun, and F. Nori, Phys. Rev. Lett. **101**, 100501 (2008); L. Zhou, H. Dong, Y. X. Liu, C. P. Sun, and F. Nori, Phys. Rev. A **78**, 063827 (2008).

[25] J. Q. Liao, Z. R. Gong, L. Zhou, Y. X. Liu, C. P. Sun, and F. Nori, e-print arXiv:0909.2748.

[26] J. Q. You and F. Nori, Phys. Rev. B **68**, 064509 (2003); J. Q. You, J. S. Tsai, and F. Nori, *ibid.* **68**, 024510 (2003).

[27] A. Wallraff, D. I. Schuster, A. Blais, L. Frunzio, R.-S. Huang, J. Majer, S. Kumar, S. M. Girvin, and R. J. Schoelkopf, Nature (London) **431**, 162 (2004).

[28] Y. X. Liu, L. F. Wei, and F. Nori, Europhys. Lett. **67**, 941 (2004).

[29] M. Hofheinz, E. M. Weig, M. Ansmann, R. C. Bialczak, E. Lucero, M. Neeley, A. D. O'Connell, H. Wang, J. M. Martinis, and A. N. Cleland, Nature (London) **454**, 310 (2008).

[30] M. Hofheinz *et al.*, Nature (London) **459**, 546 (2009).

[31] A. A. Abdumalikov Jr., O. Astafiev, Y. Nakamura, Y. A. Pashkin, and J.-S. Tsai, Phys. Rev. B **78**, 180502(R) (2008).

[32] Y. R. Shen, *The Principles of Nonlinear Optics* (Wiley, New York, 2003).

[33] G. Ithier *et al.*, Phys. Rev. B **72**, 134519 (2005).

[34] J. Hauss, A. Fedorov, S. Andre, V. Brosco, C. Hutter, R. Kothari, S. Yeshwanth, A. Shnirman, and G. Schön, New J. Phys. **10**, 095018 (2008).

[35] F. Bloch, Phys. Rev. **105**, 1206 (1957); A. G. Redfield, IBM J. Res. Dev. **1**, 19 (1957).

[36] S. Ashhab, J. R. Johansson, A. M. Zagoskin, and F. Nori, New J. Phys. **11**, 023030 (2009).

[37] C. M. Wilson, G. Johansson, T. Duty, F. Persson, M. Sandberg, and P. Delsing, Phys. Rev. B **81**, 024520 (2010).

[38] T. Duty, D. Gunnarsson, K. Bladh, and P. Delsing, Phys. Rev. B **69**, 140503(R) (2004).

[39] F. Yoshihara, K. Harrabi, A. O. Niskanen, Y. Nakamura, and J. S. Tsai, Phys. Rev. Lett. **97**, 167001 (2006).